

The ANITA Anomalous Events and Axion Quark Nuggets

Xunyu Liang and Ariel Zhitnitsky

Department of Physics and Astronomy, University of British Columbia, Vancouver, V6T 1Z1, BC, Canada

The Antarctic Impulse Transient Antenna (ANITA) collaboration [1–3] have reported observation of two anomalous events with noninverted polarity. These events are proven to be hard to explain in terms of conventional cosmic rays (CR). We propose that these anomalous events represent the direct manifestation of the dark matter (DM) annihilation events within the so-called axion quark nugget (AQN) DM model, which was originally invented for completely different purpose to explain the observed similarity between the dark and the visible components in the Universe, i.e. $\Omega_{\text{DM}} \sim \Omega_{\text{visible}}$ without any fitting parameters. We support this proposal by demonstrating that the observations [1–3], including the frequency, intensity and time duration of the radio pulses nicely match the emission features of the upward going AQN events. We list a number of features of the AQN events which are very distinct from conventional CR air showers. The observations (non-observation) of these features may substantiate (refute) our proposal.

I. INTRODUCTION

The ANITA collaboration have reported [1–3] observation of two anomalous events that appear to be energetic cosmic showers emerging from the Earth with large exit angles. We overview the corresponding events below in details. We also highlight some difficulties in interpretation of these events in terms of the standard model (SM) physics and in terms of beyond-the-SM (BSM) physics. Specifically, some BSM explanations were proposed exclusively with a single goal to explain the observed ANITA anomalous events (AAEs).

In the present work we advocate an alternative idea that the ANITA anomalous events could be a direct consequence of the axion quark nugget (AQN) model which was invented long ago without any relation to the ANITA observations. Rather, it was invented to explain the observed similarity between the DM and the visible densities in the Universe, i.e. $\Omega_{\text{DM}} \sim \Omega_{\text{visible}}$ without any fitting parameters. Nevertheless, we will argue in this work that the observations [1–3], including the frequency, intensity and time duration of the radio pulses can be explained in terms of the upward (Earth-emergent) AQN events. It is important to emphasize that the relevant parameters of the model have been fixed long ago for completely different purposes in a very different context in dramatically different systems, without any references to the ANITA anomalous events. It should be contrasted with many recent proposals when specific BSM fields and interactions were specifically introduced to match the observations.

To date, the ANITA experiment has completed four flights [1–3] and reported two anomalously steeply upward-going, radio-detected CR-like air shower events that is compatible with a ν_τ neutrino interpretation of energy \sim EeV at exit angles of -27° and -35° relative to horizontal in the first [1] and third [2] flights respectively. The radio pulse of an ANITA anomalous event observed by the ANITA balloon payload at an altitude of ~ 35 km is of order $(0.1 - 1)$ mV/m in electric field strength and $(1-10)$ ns in time duration. The observed frequency spec-

trum of the signal is in range $(40 - 800)$ MHz, and attenuates sharply beyond the critical frequency near 800 MHz.

Now we overview some suggestions [4–30] to explain the ANITA anomalous events. We also mention some of the difficulties which occur with many of these proposals.

The AAEs are in critical tension with the standard model because neutrinos is exceedingly unlikely to traverse through Earth at a distance of $\gtrsim 5 \times 10^3$ km with such ultrahigh energy, even accounting for the ν_τ regeneration [1]. The analysis [5] reviewed the high-energy neutrino events from the IceCube Neutrino Observatory and inferred that the ν_τ interpretation is excluded by at least 5σ confidence. Similar study in Ref. [6] estimated ANITA acceptance to a ν_τ flux, and concluded an at least two orders of magnitude above the upper limit from Pierre Auger Observatory and IceCube. More recently, IceCube also published severe constraints of astrophysical explanation for the AAEs under SM assumptions [30].

Alternative explanations such as transition radiation [4, 10] remains unconfirmed, and some are either disfavoured [8] or largely excluded by ANITA [13, 15]. Notably, several BSM explanations are proposed [7, 9, 11, 14, 16–29]. In most cases, it suggests an origin of a (or a group of) massive hypothetical particle(s), which is strongly constrained by the IceCube and Auger bounds [12]. The other common problem is that the models are largely fine-tuned to match the observation of the AAEs and lack of a natural motivation.

In the present work we put forward a proposal that the AAEs could be a direct consequence of the AQN model [31]. The model was originally invented to explain the observed similarity between the DM and the visible densities in the Universe, see Sec. II with more details on the model. The important feature of our proposal is that the AQN model involves no fine-tuning of parameters because this model is not devised to match the observation of AAEs, but rather its properties are well studied and constrained by numerous unrelated phenomena in the previous studies. Our presentation is organized as follows. In subsection II A we overview the basics of the AQN model, while in subsections II B and II C we overview the features of the AQN model which will be

relevant for the present work. We formulate our proposal on identification of AAE with AQN upward-going events in Sec. III, while in Sec. IV we estimate the corresponding event rate and in Sec V we carry out explicit computations of the spectral properties of the radio pulse and estimate the intensity, which support our interpretation of the AAEs as Earth-emergent AQN events. We conclude with Sec. VI where we explicitly formulate some dramatic differences between AQN events and conventional CR events. We also suggest possible tests which may support or refute our proposal.

II. THE AQN DM MODEL

We start with few historical remarks and motivation of the AQN model in subsection II A, while in subsection II B we overview recent observations (such as puzzling bursts observed by the Telescope Array experiment) of some mysterious events which could be explained by the AQN events hitting the Earth. Finally, in section II C we overview some specific features of the AQNs traversing the Earth (such as internal temperature, level of ionization, etc). These characteristics will be important for the present study interpreting the ANITA anomalous events as the Earth-emergent AQN events.

A. The basics

The AQN DM model [31] was invented long ago with a single motivation to naturally explain the observed similarity between the DM and the visible densities in the Universe, i.e. $\Omega_{\text{DM}} \sim \Omega_{\text{visible}}$ without any fitting parameters. The AQN construction in many respects is similar to the Witten’s quark nuggets, see [32–34], and review [35]. This type of DM is “cosmologically dark” not because of the weakness of the AQN interactions, but due to their small cross-section-to-mass ratio, which scales down many observable consequences of an otherwise strongly-interacting DM candidate.

There are two additional elements in the AQN model compared to the original models [32–35]. First new element is the presence of the axion domain walls which are copiously produced during the QCD transition¹. This domain wall plays a dual role: first it serves as an additional stabilization factor for the nuggets, which helps to alleviate a number of problems with the original nugget

construction [32–35]. Secondly, the same axion field $\theta(x)$ generates the strong and coherent \mathcal{CP} violation in the entire visible Universe.

This is because the $\theta(x)$ axion field before the QCD epoch could be thought as classical \mathcal{CP} violating field correlated on the scale of the entire Universe. The axion field starts to oscillate at the QCD transition by emitting the propagating axions. However, these oscillations remain coherent on the scale of the entire Universe. Therefore, the \mathcal{CP} violating phase remains coherent on the same enormous scale.

Another feature of the AQN model which plays absolutely crucial role for the present work is that nuggets can be made of *matter* as well as *antimatter* during the QCD transition. Precisely the coherence of the \mathcal{CP} violating field on large scale mentioned above provides a preferential production of one species of nuggets made of *antimatter* over another species made of *matter*. The preference is determined by the initial sign of the θ field when the formation of the AQN starts. The direct consequence of this feature along with coherent \mathcal{CP} violation in entire Universe is that the DM density, Ω_{DM} , and the visible density, Ω_{visible} , will automatically assume the same order of magnitude densities $\Omega_{\text{DM}} \sim \Omega_{\text{visible}}$ without any fine tuning. We refer to the original papers [52–55] devoted to the specific questions related to the nugget’s formation, generation of the baryon asymmetry, and survival pattern of the nuggets during the evolution in early Universe with its unfriendly environment.

One should emphasize that AQNs are absolutely stable configurations on cosmological scales. Furthermore, the antimatter which is hidden in form of the very dense nuggets is unavailable for annihilation unless the AQNs hit the stars or the planets.

However, when the AQNs hit the stars or the planets it may lead to observable phenomena. In particular, the injection of the energy due to the AQNs hitting the Sun may explain² the “Solar Corona heating problem” as advocated in [58–60]. There are also very rare events of annihilation in the center of the galaxy, which, in fact, may explain some observed galactic excess emissions in different frequency bands, including famous 511 keV line.

The strongest direct detection limit³ is set by the Ice-

¹ The axion field had been introduced into the theory to resolve the so-called the strong \mathcal{CP} problem which is related to the fundamental initial parameter $\theta_0 \neq 0$. This source of \mathcal{CP} violation is no longer available at the present time as a result of the axion’s dynamics in early Universe. One should mention that the axion remains the most compelling resolution of the strong \mathcal{CP} problem, see original papers on the axion [36–42], and recent reviews [43–51].

² In fact, to resolve this problem Parker conjectured long ago [56] that “nanoflares” are identified with the annihilation events in the AQN framework. The luminosity of the Extreme UV (EUV) radiation from corona due to these annihilation events is unambiguously determined by the DM density. It is very nontrivial consistency check that the computed luminosity from the corona nicely matches with observed EUV radiation. The same events of annihilation are also manifested themselves as the radio impulsive events in quiet solar corona as recently recorded by Murchison Widefield Array Observatory [57], which also represents a very nontrivial consistency check of the proposal [58, 59] on the “Solar Corona Mystery” resolution and accompanying radio impulsive events in quiet solar corona [60].

³ Non-detection of etching tracks in ancient mica gives another

Cube Observatory’s, see Appendix A in [62]:

$$\langle B \rangle > 3 \cdot 10^{24} \quad [\text{direct (non)detection constraint}]. \quad (1)$$

Similar limits are also obtainable from the ANITA and from geothermal constraints which are also consistent with (1) as estimated in [63]. It has been also argued in [64] that AQNs producing a significant neutrino flux in the 20-50 MeV range cannot account for more than 20% of the DM density. However, the estimates [64] were based on assumption that the neutrino spectrum is similar to the one which is observed in conventional baryon-antibaryon annihilation events which typically produce a large number of pions and muons and thus generate a significant number of neutrinos and antineutrinos in the 20-50 MeV range where SuperK has a high sensitivity. However, the critical difference in the case of AQNs is that the annihilation proceeds within the colour superconducting (CS) phase where the energetics are drastically different [65]. The main point is that, in most CS phases, the lightest pseudo Goldstone mesons (the pions and kaons) have masses in the 20 MeV range, rather than 140 MeV in hadronic phase. This dramatically changes entire spectrum such that the main assumption of [64] on similarity of the neutrino’s spectrum in both phases is incorrect. The resulting flux computed in [65] is perfectly consistent with observations. Furthermore, precisely these low energy ($\lesssim 20$ MeV) AQN-induced neutrinos produced in the Earth’s interior might be responsible for explanation of the long standing puzzle of the DAMA/LIBRA observation of the annual modulation at 9.5σ confidence level as argued in [66].

The authors of Ref. [67] considered a generic constraint for the nuggets made of antimatter (ignoring all essential specifics of the AQN model such as quark matter CS phase of the nugget’s core). Our constraints (1) are consistent with their findings including the Cosmic Microwave Background (CMB), Big Bang Nucleosynthesis (BBN), and others, except the constraints derived from the so-called “Human Detectors”. As explained in [60] the corresponding estimates of Ref. [67] are oversimplified and do not have the same status as those derived from CMB or BBN constraints⁴.

indirect constraint on the flux of DM nuggets with mass $M < 55g$ [61]. This constraint is based on assumption that all nuggets have the same mass, which is not the case as we discuss below. The nuggets with small masses represent a tiny portion of all nuggets in this model, such that this constraint is easily satisfied with any reasonable nugget’s size distribution.

⁴ In particular, the rate of energy deposition was estimated in [67] assuming that the annihilation processes between antimatter nuggets and baryons are similar to $p\bar{p}$ annihilation process. It is known that it cannot be the case because the annihilating objects have drastically different internal structures (hadronic phase versus CS phase). It has been also assumed in [67] that a typical X ray energy is around 1 keV, which is much lower than direct computations in the AQN model would suggest [68]. Higher energy X rays have much longer mean free path, which implies that

While ground based direct searches offer the most unambiguous channel for the detection of quark nuggets the flux of nuggets is inversely proportional to the nugget’s mass and consequently even the largest available conventional DM detectors are incapable to exclude the entire potential mass range of the nuggets. Instead, the large area detectors which are normally designed for analysing the high energy cosmic rays are much better suited for our studies of the AQNs as we discuss in next section II B.

B. When the AQNs hitting the Earth...

For our present work, however, the most relevant studies are related to the effects which may occur when the AQNs made of antimatter hit the Earth and continue to propagate in deep underground in very dense environment. In this case the most of the energy injection will occur in the Earth’s interior. The corresponding signals are very hard to detect as the photons, electrons and positrons will be quickly absorbed by surrounding dense material deep underground, while the emissions of the very weakly interacting neutrinos and axions are hard to recover. Nevertheless, as we already mentioned, the AQN-induced neutrinos produced in the Earth’s interior might be responsible for explanation of the long standing puzzle of the DAMA/LIBRA observation of the annual modulation [66]. The AQN-induced axions from deep interior can be recovered by analyzing the daily and annual modulations as suggested in [69] and elaborated in [70]. The AQN annihilation events in the Earth’s atmosphere could produce infrasound and seismic acoustic waves as discussed in [68, 71] when the infrasound and seismic acoustic waves indeed have been recorded by dedicated instruments⁵. Furthermore, the AQN annihilation

the dominant portion of the energy will be deposited outside the human body. Finally, the authors of Ref. [67] assume that an antimatter nugget will result in “injury similar to a gunshot”. It is obviously a wrong picture as the size of a typical nugget is only $R \sim 10^{-5}cm$ while the most of the energy is deposited in form of the X rays on centimeter scales [68] without making a large hole similar to bullet as assumed in [67]. In this case a human’s death may occur as a result of a large dose of radiation with a long time delay, which would make it hard to identify the cause of the death. This argument (about the time delay and difficulties with possible death identification) should be contrasted with the main assumption of [67] that all such cases would be unambiguously and quickly identified. While in the journal version of [67] the constraint had been weakened in comparison with the arXiv version, we still think it is not adequately reflect the complex physics as outlined above.

⁵ A single observed event properly recorded by the Elginfield Infrasound Array (ELFO) which was accompanied by correlated seismic waves is dramatically different from conventional meteor-like events. In particular, while the event was very intense it has not been detected by a synchronized all-sky camera network (visible frequency bands) which ruled out a meteor source. At the same time this event is consistent with interpretation of the

events may explain the mysterious bursts (representing a cluster of 3+ individual cosmic ray-like events) observed by Telescope Array (TA) experiment [72, 73] in terms of the AQN annihilation events under the thunderstorm⁶ as argued in [74, 75].

Finally, the seasonal variations of the X ray background in the near-Earth environment in the 2-6 keV energy range as observed by the XMM-Newton at 11σ confidence level [76] may be also naturally explained within the same AQN framework as argued [77]. This application to the X ray emission in the near-Earth environment is especially relevant for the present work because the AQN-induced X rays according to the proposal [77] are originated from the AQN upward (Earth emergent) events when the AQNs traversed through the Earth interior and exit the Earth surface. Such events could, in principle, be responsible for the ANITA mysterious events [1–3] with exit angles of -27° and -35° relative to the horizon as advocated in present work. Before we present our arguments in next section we have to highlight the basic characteristics of the AQNs traversing the Earth, which is the topic of the next subsection.

C. Upward (Earth-emergent) events

The goal here is to explain the basic features of the AQNs when they enter the dense regions of the surrounding material and annihilation processes start. The related computations originally have been carried out in [78] in application to the galactic environment with a typical density of surrounding visible baryons of order $n_{\text{galaxy}} \sim 300 \text{ cm}^{-3}$ in the galactic center, in dramatic contrast with dense region in the Earth's interior when $n_{\text{rock}} \sim 10^{24} \text{ cm}^{-3}$. We review these computations with few additional elements which must be implemented in case of propagation in the Earth's atmosphere and interior when the density of the environment is much greater than in the galactic environment.

The total surface emissivity from electrosphere has

been computed in [78] and it is given by

$$F_{\text{tot}} \approx \frac{16}{3} \frac{T^4 \alpha^{5/2}}{\pi} \sqrt[4]{\frac{T}{m}}, \quad (2)$$

where $\alpha \approx 1/137$ is the fine structure constant, $m = 511 \text{ keV}$ is the mass of electron, and T is the internal temperature of the AQN. One should emphasize that the emission from the electrosphere is not thermal, and the spectrum is dramatically different from blackbody radiation, see [78], see also Appendix A with more details.

A typical internal temperature of the AQNs for very dilute galactic environment can be estimated from the condition that the radiative output of Eq. (2) must balance the flux of energy onto the nugget

$$F_{\text{tot}}(4\pi R^2) \approx \kappa \cdot (\pi R^2) \cdot (2 \text{ GeV}) \cdot n \cdot v_{\text{AQN}}, \quad (3)$$

where n represents the number density of the environment. The left hand side accounts for the total energy radiation from the AQN's surface per unit time as given by (2) while the right hand side accounts for the rate of annihilation events when each successful annihilation event of a single baryon charge produces $\sim 2m_p c^2 \approx 2 \text{ GeV}$ energy. In Eq. (3) we assume that the nugget is characterized by the geometrical cross section πR^2 when it propagates in environment with local density n with velocity $v_{\text{AQN}} \sim 10^{-3}c$.

The factor κ is introduced to account for the fact that not all matter striking the AQN will annihilate and not all of the energy released by an annihilation will be thermalized in the AQNs by changing the internal temperature T . In particular, some portion of the energy will be released in form of the axions, neutrinos and electron-positron pairs by the mechanism discussed below. In a neutral dilute environment considered previously [78] the value of κ cannot exceed $\kappa \lesssim 1$ which would correspond to the total annihilation of all impacting matter into thermal photons. The high probability of reflection at the sharp quark matter surface lowers the value of κ . The propagation of an ionized (negatively charged) nugget in a highly ionized plasma (such as solar corona) will increase the effective cross section. As a consequence, the value of κ could be very large as discussed in [59] in application to the solar corona heating problem.

The internal AQN temperature had been estimated previously for a number of cases. It may assume dramatically different values, mostly due to the huge difference in number density n entering (3). In particular, for the galactic environment $T_{\text{galaxy}} \approx 1 \text{ eV}$, while in deep Earth's interior it could be as high as $T_{\text{rock}} \approx (100 - 200) \text{ keV}$. Precisely this value of T had been used as initial temperature of the nuggets in the proposal [77] explaining the seasonal variations of the X rays observed by the XMM-Newton at 11σ confidence level [76] at distances $r \sim (6 - 10)R_\oplus$ from the Earth surface. For our estimates in the present work we shall use the same $T_{\text{rock}} \approx (100 - 200) \text{ keV}$ for explaining the ANITA anomaly.

AQN-induced event because the visible frequency bands must be strongly suppressed when AQN propagates in atmosphere [68]

⁶ These events are very unusual and cannot be interpreted in terms of conventional cosmic ray (CR) single showers. In particular, if one tries to fit the observed bursts (cluster events) with conventional code, the energy for CR events should be in 10^{13} eV energy range to match the frequency of appearance, while the observed bursts correspond to $(10^{18} - 10^{19}) \text{ eV}$ energy range as estimated by signal amplitude and distribution. Therefore, the estimated energy from individual events within the bursts is five to six orders of magnitude higher than the energy estimated by event rate [72, 73]. Furthermore, the bursts events do not have sharp edges in waveforms in comparison with conventional CR events. Also, all 10 recorded bursts occur under thunderstorm, which is very hard to interpret in terms of the conventional cosmic rays events which should not be modified by low-energy physics of thunderclouds.

lous events⁷. The difference with previous studies [77] is that in this work we are interested in the instant when the very hot AQNs just cross the Earth surface and enter the atmosphere (upward events). As we argue below the radio pulse is emitted precisely at this moment. It should be contrasted with the applications considered in [77] when the nuggets had travelled $\sim 10^4$ km in empty space before emitted X rays could be detected by XMM-Newton observatory.

One more feature we want to mention here which is relevant for our studies is the ionization property. Ionization, as usual, may occur in the system as a result of the high internal temperature T discussed above. To be more precise, the high internal temperature T excites a large number of positrons $\sim Q$ from electrosphere. These positrons are weakly bound particles which can easily leave the system. The corresponding parameter Q can be estimated as follows:

$$Q \approx 4\pi R^2 \int_0^\infty n(z, T) dz \sim \frac{4\pi R^2}{\sqrt{2\pi\alpha}} (mT) \left(\frac{T}{m}\right)^{\frac{1}{4}}, \quad (4)$$

where $n(z, T)$ is the local density of positrons at distance z from the nugget's surface, which has been computed in the mean field approximation in [78, 79] and has the following form

$$n(z, T) = \frac{T}{2\pi\alpha} \frac{1}{(z + \bar{z})^2}, \quad (5)$$

where \bar{z} is the integration constant is chosen to match the Boltzmann regime at sufficiently large $z \gg \bar{z}$. Numerical studies [79] support the approximate analytical expression (5).

$$\bar{z}^{-1} \approx \sqrt{2\pi\alpha} \cdot m \cdot \left(\frac{T}{m}\right)^{\frac{1}{4}}, \quad n(z=0) \approx (mT)^{\frac{3}{2}}. \quad (6)$$

In the equilibrium with small annihilation rate the positrons will normally occupy very thin layer of order \bar{z} around the AQN's quark core as computed in [78, 79]. However, in our case when the AQN enters the Earth's atmosphere and further the interior a large number of non-equilibrium processes (such as generation of the shock wave as a result of large Mach number M) are expected to occur. Furthermore, the positron's cloud is expected to expand well beyond the thin layer around the core's nugget as a result of the direct collisions with atmospheric molecules, in which case some positrons will be kicked off and leave the system.

In what follows we assume that, to first order, the finite portion of positrons $\sim Q$ leave the system as a result

of these complicated processes, in which case the AQN as a system acquires a negative electric charge $\sim -|e|Q$ and get partially ionized, see also Appendix A with more details.

III. ANITA ANOMALOUS EVENTS AS AQN EARTH-EMERGENT EVENTS

With these preliminary comments from previous section on the AQN features we are now in position to formulate the proposal interpreting the ANITA anomalous events in terms of the upward moving AQNs. We refer to some technical details to the Appendix A, while here we highlight the basic idea which goes as follows.

The AQNs which propagate in the Earth's interior are very hot. Their temperature could be as hot as $T \approx (100 - 200)$ keV as we discussed in [77] in the application to studies of the seasonal variations of the X rays observed by XMM-Newton at very large distances from Earth, see footnote 7. At such large distances the AQNs (which traversed the Earth and continued to travel in empty space) are already sufficiently cold and emit mostly X rays with well defined spectrum. It should be contrasted with our present studies when we are interested in the same AQNs at the instant when the AQNs just crossed the surface and entered the Earth's atmosphere (upward-going events). It is expected that these AQNs are still very hot with $T \approx (100 - 200)$ keV, and their main cooling mechanism at the instant of surface's crossing remains the same (e^+e^- pair production).

Exactly at this instant the electrons experiencing the repulsion force due to AQNs unscreened (negative) electric charge (4) which represents inevitable feature of the AQNs with high internal temperature T . The numerical value of the charge can be estimated as (A2) where electric field is very large. This electric field may accelerate the produced electrons to very high energy $\langle E \rangle \sim 10$ MeV as given by (A13). The same electric field has opposite effect for positrons when the produced positrons will experience the attractive force and will assume a location close to the nugget's surface. One should emphasize that the positrons produced by such mechanism have dramatically different properties from the positrons from electrosphere (A1) with much smaller bound energies and which could be localized far away from the AQN's surface⁸. One should mention here that the instant when AQN crosses the boundary is very unique in a sense that all the characteristics of the AQN (the internal temperature, the pressure, the Mach number $M = v_{\text{AQN}}/c_s \gg 1$, where c_s is the speed of sound in a given environment)

⁷ It is very unlikely for the temperature to reach much higher values because a different cooling mechanism (e^+e^- pair production) becomes very efficient as T reaches the region which is relatively close to $m = 511$ keV such that the anticipated suppression $\exp(-m/T)$ becomes less dramatic for $T \gtrsim 10^2$ keV as we discuss in Appendix A.

⁸ Precisely those weakly bound positrons could be kicked off as a result of the elastic collisions with atmospheric molecule, which was the topic of the proposal [74] interpreting the mysterious burst events detected by the Telescope Array Experiment as the AQN events under a thunderstorm.

remain the same as the AQN had before the crossing in a course of propagation in dense Earth's interior with the density $n_{\text{rock}} \sim 10^{24} \text{ cm}^{-3}$. At the moment of crossing the AQN suddenly enters a new environment with dramatically different density $n_{\text{air}} \sim 10^{21} \text{ cm}^{-3}$.

We expect that the result of this instant characterized by the dramatic perturbation will be the emission of energetic electrons with typical energy $\langle E \rangle \sim 10 \text{ MeV}$ as given by (A13). One should emphasize that such radiation of photons (and accompanied emission of the e^+e^- pairs) is expected to be the dominant cooling mechanism for the AQN propagating in the deep interior before the crossing. There are two new elements (in comparison with a case when the AQNs propagate in deep interior with approximately constant density) which occur at the instant when the AQNs cross the hard surface and enter the Earth's atmosphere: 1. the emitted energetic electrons can propagate for several kilometres in atmosphere being the source of the geosynchrotron radiation, i.e. they can produce observable effects to be measured, in contrast with propagation in deep underground when the photons and the electrons will be quickly absorbed; 2. the electrons are mostly emitted in the direction of the AQN velocity at the instant of very short imbalanced pressure at the moment of crossing.

Any precise computation of this instant of crossing is very hard problem of non-equilibrium dynamics, which is beyond the scope of the present work. Fortunately, the observable radio signal (which is a result of the emitted electrons) is not very sensitive to the details of this non-equilibrium mechanism and corresponding time scales as it depends on several basic parameters such as typical energy $\langle E \rangle \sim 10 \text{ MeV}$ of the emitted electrons as estimated in (A13). Another parameter which enters all our formulae below is the number of emitted electrons N which generates a coherent radio signal. The parameter N determines the intensity of the radiation, and cannot be computed from the first principles due to the very large uncertainties of the complicated non-equilibrium dynamics such as turbulence, shock waves, strong ionization as mentioned above and further elaborated in Appendix A. We treat this parameter as a phenomenological unknown parameter which must satisfy constraint $N \ll N_{\text{max}}$ where N_{max} is the maximal number of potentially available electrons (A11) which could be, in principle, liberated from the AQN at the instant of crossing the Earth's surface.

The number of electrons N which are emitted by a conventional cosmic ray showers of energy $E_{\text{CR}} \sim (10^{17} - 10^{18}) \text{ eV}$ is of order $N \sim (10^8 - 10^9)$. We anticipate a similar magnitude for the number of electrons $N \sim (10^8 - 10^9)$ emitted by AQNs as the observed intensity of the field strength for the anomalous ANITA events of order mV/m which agrees with the value of N assuming the shower energy is $E_{\text{CR}} \sim (10^{17} - 10^{18}) \text{ eV}$.

In context of our work the value of N is treated as the phenomenological unknown parameter, as we already mentioned. It must be much smaller than N_{max} which

can be estimated (A11). Important arguments supporting our proposal that the AQN induced events could mimic the anomalous radio signals observed by ANITA are based on very specific qualitative characteristics such as the spectrum and pulse time duration, rather than on a precise estimation of parameter N . The event rate of such anomalous events is also shown to be consistent with our AQN-based interpretation, see next section IV.

Furthermore, the average electron's energy in the energetic CR events with $E_{\text{CR}} \sim (10^{17} - 10^{18}) \text{ eV}$ is around 30 MeV which is in the same energy range of the AQN-induced electrons as estimated in (A13). Therefore, the electrons which are released as a result of AQN crossing the boundary in upward (Earth emergent) event could mimic the radio signal of the conventional CR shower events as detected by ANITA. The estimation of the specific properties of the AQN-induced radio signal such as the spectrum, time pulse duration and the intensity is the topic of Sec. V.

IV. EVENT RATE OF AAE

This section is devoted to estimate the event rate of AAEs within the AQN framework. It is expected to be a qualitative estimate up to an order-of-magnitude check due to large uncertainties in parameters and rare occurrence of the observed AAEs. Nevertheless we would like to present such estimate to demonstrate that our interpretation of AAEs as a consequence of upward-going AQNs is at least a self-consistent proposal.

The expected number of the AAEs assuming that they are induced by the AQNs can be estimated as follows:

$$\mathcal{N} \approx \mathcal{A}_{\text{eff}} \mathcal{T} \Delta \Omega \frac{d\Phi}{dAd\Omega}, \quad (7)$$

where $\mathcal{A}_{\text{eff}} \approx 4 \text{ km}^2$ is the effective area of ANITA [2], $\mathcal{T} \approx 48.75 \text{ days}$ is the combined exposure time of ANITA⁹, $\Delta \Omega \approx 2\pi$ for isotropic flux of AQNs, Φ is the total hit rate of AQNs on Earth [62]:

$$\begin{aligned} \Phi &\approx 2.12 \times 10^7 \text{ yr}^{-1} \\ &\times \left(\frac{\rho_{\text{DM}}}{0.3 \text{ GeV cm}^{-3}} \right) \left(\frac{v_{\text{AQN}}}{220 \text{ km s}^{-1}} \right) \left(\frac{10^{25}}{\langle B \rangle} \right), \end{aligned} \quad (8)$$

where ρ_{DM} is the local density of DM. The local rate of upward-going AQNs per unit area depends on the flux distribution of the AQN:

$$\frac{d\Phi}{dAd\Omega} = \frac{\eta}{4\pi R_{\oplus}^2} \Phi = 4 \cdot 10^{-2} \left(\frac{10^{25}}{\langle B \rangle} \right) \frac{\eta \text{ events}}{\text{yr} \cdot \text{km}^2} \quad (9)$$

⁹ The effective exposure time was 17.25 days for ANITA-I [80], 7 days for ANITA-III [2], and 24.5 days for ANITA-IV [3], where we exclude ANITA-II (28.5 days) as it is not sensitive to upward-going air showers.

where $R_{\oplus} = 6371$ km is the radius of the Earth, and η is a parameter that characterizes the local flux distribution of AQN. Specifically, $\eta \approx 1$ for isotropic distribution, and $\eta \approx 2$ for the so-called fixed-wind distribution based on standard halo model so that more AQNs enter the Earth from the northern hemisphere and exit in the southern hemisphere [81]. Note that the survival rate of an AQN traverses through Earth is also taken into account in η implicitly, but it is an exceedingly minor effect comparing to the flux distribution because AQNs can penetrate through the Earth easily based on Monte Carlo simulation in Ref. [62].

Combining the estimates above, one should have

$$\mathcal{N} \approx 0.28 \left(\frac{\eta}{2} \right) \left(\frac{\rho_{\text{DM}}}{0.3 \text{ GeV cm}^{-3}} \right) \left(\frac{v_{\text{AQN}}}{220 \text{ km s}^{-1}} \right) \left(\frac{10^{25}}{\langle B \rangle} \right). \quad (10)$$

The expected number of events $\mathcal{N} \approx 0.3$ is almost one order of magnitude lower than $\mathcal{N}_{\text{obs}} = 2$ events observed by ANITA. Nevertheless, we consider this order of magnitude estimation (10) being consistent with our proposal due to many uncertainties which enter this estimate.

First, the parameters in Eq. (10) are in fact not precisely known. Essential parameters such as η , ρ_{DM} , $\langle v_{\text{AQN}} \rangle$, and $\langle B \rangle$ only have accuracy up to order one as the local flux distribution of DM and size distribution of AQN remain unknown to date. In fact, there are numerous hints suggesting that ρ_{DM} locally in solar system could be much larger from its canonical value, see a short comment on this with the references in the last paragraph of this section. Similarly, the effective area of detection \mathcal{A}_{eff} may double depending on the exit angle (see estimate in e.g. Ref. [18]), and the effective exposure time is potentially longer than our conservative estimate if we take into account the ANITA-II flight in the estimate (see footnote 9). In addition, the total number of observed AAEs could be a statistical fluctuation due to its rare occurrence (only 2).

We consider this order of magnitude estimate (10) as a highly nontrivial consistency check of our proposal as the basic numerical factors entering (10) had been fixed from dramatically different physics (including solar corona heating puzzle) and can easily deviate by large factor. More importantly, our main arguments leading to the identification of the AAE with the AQN induced radio pulses are based on specific qualitative features such as frequency dependence and duration of the pulse which are not sensitive to these huge uncertainties in the normalization factor (10). We consider the agreement between the observations and our theoretical estimates (to be discussed in next section V) for these specific characteristics as the strong arguments supporting our identification.

It is also interesting to note that the extra numerical factor 0.1 (between computed and observed values) which appears in our order of magnitude estimates (10) is very similar to extra factor 0.1 which occurred in analogous computations [74] of a number of mysterious bursts observed by the Telescope Array. This similarity hints on

a common origin of both phenomena though the physics for these two phenomena are dramatically different. This is because the main normalization factor representing the DM flux in the form of the AQN induced events (9) is identically the same for both estimates, for AAE (10) and for Telescope Array mysterious event count [74]. If future studies support our identification of the AAE with the AQN induced radio pulses this numerical suppression factor might be a hint that the Standard Halo Model (which is used in estimations for the DM flux) underestimates the local DM density in solar system. The true DM density locally may dramatically deviate from average global value $\rho_{\text{DM}} \approx 0.3 \text{ GeV cm}^{-3}$, see Introduction in [70] for the references and details.

V. RADIO SIGNALS INDUCED BY AQN

It is well known that the frequency spectrum of geosynchrotron radiation by an ultrarelativistic charged particle is equivalent to that emitted by a particle moving instantaneously at constant speed on an appropriate circular path with instantaneous radius of curvature ρ , see e.g. Jackson [82]:

$$\rho \approx \frac{\gamma mc}{e\mathcal{B} \sin \theta_{\mathcal{B}}} \approx 0.8 \text{ km} \left(\frac{\gamma}{20} \right), \quad (11)$$

where $\mathcal{B} \approx 0.5$ gauss is the local magnetic field strength, and $\theta_{\mathcal{B}}$ is the angle between the particle velocity \mathbf{v} and magnetic direction. We choose $\theta_{\mathcal{B}} \approx 60^\circ$ in this work, as the magnetic field direction in Antarctica is approximately vertical and the exit angle of the AAEs are typically of order 30° .

The geometry follows from Fig. 1, the segment of trajectories lies in the x - y plane. The θ is the observation angle between \mathbf{v} and the direction of the observer \mathbf{n} . An ultrarelativistic particle with Lorentz factor $\gamma \gg 1$ has a narrow emission angle $\theta \lesssim \gamma^{-1}$, beyond which the intensity of radiation is exponentially suppressed. The ϵ_{\parallel} and ϵ_{\perp} are the two directions of polarization as shown on Fig. 1.

For an observer with distance \mathcal{R} from N coherent charged particles, the spectral component of the electric field $\mathbf{E}(\omega)$ as a function of frequency ω is given by [82]

$$|\mathbf{E}(\omega)| = N \left(\frac{4\pi}{c} \right)^{1/2} \frac{1}{\mathcal{R}} |\mathbf{A}(\omega)|, \quad (12)$$

$$\mathbf{A}(\omega) = \frac{-ie\omega}{\sqrt{8c\pi}} [-\epsilon_{\parallel} A_{\parallel}(\omega) + \kappa \epsilon_{\perp} A_{\perp}(\omega)],$$

where $A_{\parallel}(\omega)$ and $A_{\perp}(\omega)$ corresponds to the amplitudes of two polarization directions in terms of modified Bessel functions:

$$A_{\parallel}(\omega) = i \frac{2\rho}{\sqrt{3}c} \left(\frac{1}{\gamma^2} + \theta^2 \right) K_{2/3}(\xi), \quad (13a)$$

$$A_{\perp}(\omega) = \theta \frac{2\rho}{\sqrt{3}c} \left(\frac{1}{\gamma^2} + \theta^2 \right)^{1/2} K_{1/3}(\xi), \quad (13b)$$

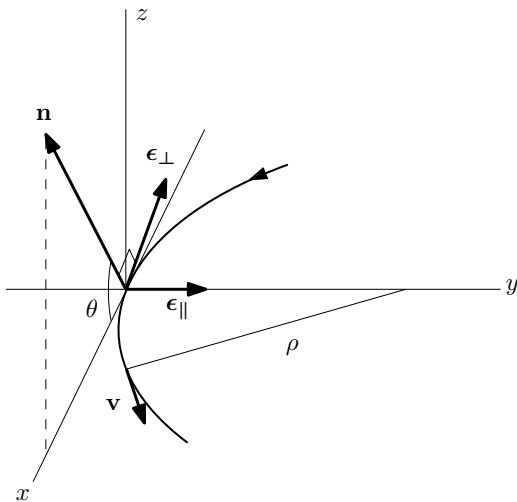


FIG. 1.

with

$$\xi = \frac{\rho\omega}{3c} \left(\frac{1}{\gamma^2} + \theta^2 \right)^{3/2}. \quad (14)$$

Note that Eqs. (13) are only well-defined for $\omega > 0$, the values in the negative domain is defined by $\mathbf{A}(-\omega) = \mathbf{A}^*(\omega)$. The parameter κ in (12) is introduced to characterize the screening effect of e^+e^- pair, where the ϵ_{\perp} -component is effectively cancelled ($\kappa \approx 0$) when e^+e^- pairs are predominantly formed in conventional CR events [83]. In the opposite limit, we choose $\kappa \approx 1$ in case of AQN-induced signal as it is primarily initiated by electrons such that the screening effect is diminished. The spectrum of electric field is therefore

$$|\mathbf{E}(\omega)| \approx \sqrt{\frac{2}{3\pi}} \frac{N\epsilon\rho\omega}{c^2\mathcal{R}} \left(\frac{1}{\gamma^2} + \theta^2 \right) K_{2/3}(\xi) \times \sqrt{1 + \frac{\gamma^2\theta^2}{1 + \gamma^2\theta^2} \left(\frac{K_{1/3}(\xi)}{K_{2/3}(\xi)} \right)^2}. \quad (15)$$

The observational distance from ANITA balloon payload is of order 35 km and the size of the detector is of order 10 m, therefore the effective observation angle is tiny comparing to the emission angle $\theta \sim 10^{-4} \ll \gamma^{-1}$.

Choosing $\theta = 0$, we plot the spectrum (15) in Fig. 2 with different values of γ for a specific value of $N = 5 \times 10^8$. One can see that the spectrum is very flat: the absolute value $|\mathbf{E}(\omega)|$ changes by a factor of 3 or so when the frequency ν varies by 2 orders of magnitude. Furthermore, the total strength of the electric field integrated over entire frequency band agrees with the observed value on the level of $|\mathbf{E}| \sim \text{mV/m}$, see Refs. [1–3].

Another generic feature of synchrotron radiation is the exponential suppression of the emission beyond the critical frequency [82]

$$\nu_c \equiv \frac{3\gamma^3 c}{4\pi\rho} \approx 0.7 \text{ GHz} \left(\frac{\gamma}{20} \right)^2. \quad (16)$$

This qualitative consequence of our proposal is also consistent with ANITA observations[1–3].

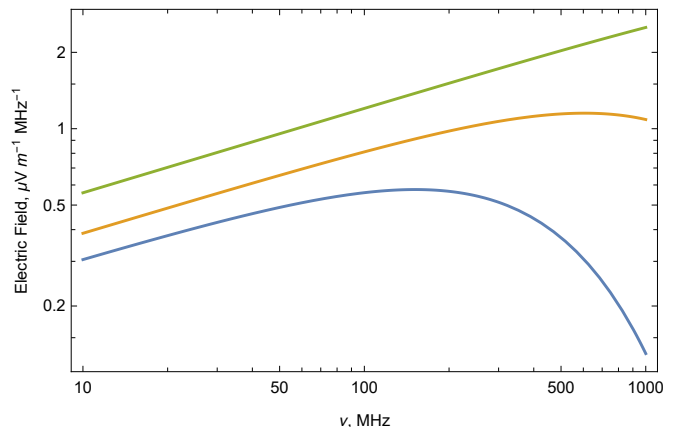


FIG. 2. Spectrum of electric field $|E(2\pi\nu)|$ from Eq. (15), with $\theta = 0$, $\mathcal{R} = 35 \text{ km}$, and $N = 5 \cdot 10^8$. The Lorentz factor is chosen to be $\gamma = 10$ (blue), 20 (orange), and 60 (green).

The time-dependent radio pulse can be reconstructed from the frequency spectrum by an inverse Fourier transform:

$$\mathbf{E}(t) = \frac{1}{\sqrt{2\pi}} \int_{-\infty}^{\infty} b(\omega) \mathbf{E}(\omega) e^{-i\omega t} d\omega \approx -\epsilon_{\parallel} \frac{2Ne\rho}{\sqrt{3\pi}c^2\gamma^2\mathcal{R}} \text{Re} \left[\int_0^{\infty} b(\omega) \omega K_{2/3}(\xi) e^{-i\omega t} d\omega \right] \quad (17)$$

where $b(\omega)$ is the filter characterizing the receiver, similar to analysis in [83]. For illustrative purpose, we plot the time-dependent electric field in Fig. 3 by assuming an idealized rectangle filter spanning (40–80) MHz and (200–600) MHz. The pulse has an amplitude $|\mathbf{E}_0| \sim \text{mV/m}$ and the time duration $\tau \sim \text{ns}$, which is consistent with observed features of the anomalous pulses observed by ANITA [1–3]. Because $|\mathbf{E}(\omega)|$ is approximately flat in frequency range below ν_c , $\mathbf{E}(t)$ is essentially determined by the inverse Fourier transform of $b(\omega)$. In case of a rectangle-like filter with frequency bandwidth $\Delta\nu$, the time duration of the pulse is determined by $\Delta\nu$ as follows:

$$\tau \approx \frac{1}{\Delta\nu} \approx 2 \text{ ns} \left(\frac{600 \text{ MHz}}{\Delta\nu} \right). \quad (18)$$

The numerical value for the time scale τ is not very sensitive to the parameters of the model as explained above due to the flatness of the spectrum below ν_c . In contrast to the time duration τ the absolute value of the electrical field $|\mathbf{E}_0| \sim \text{mV/m}$ is sensitive to γ as shown on Fig. 3. It assumes the values which are also consistent with observations [1–3].

It is instructive to understand the temporal features of the electric field $\mathbf{E}(t)$ by rewriting the integral (17) in terms of the dimensionless variable ξ defined by (14) as

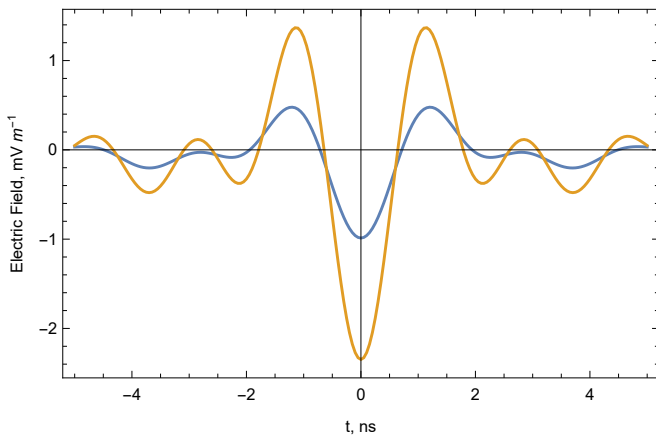


FIG. 3. Time-dependent electric field from Eq. (17) with $\theta = 0$, $\mathcal{R} = 35$ km, and $N = 5 \cdot 10^8$, using an idealized rectangle filter. The Lorentz factor is chosen to be $\gamma = 10$ (blue) and 20 (orange); filter: (40-80) MHz and (200-600) MHz.

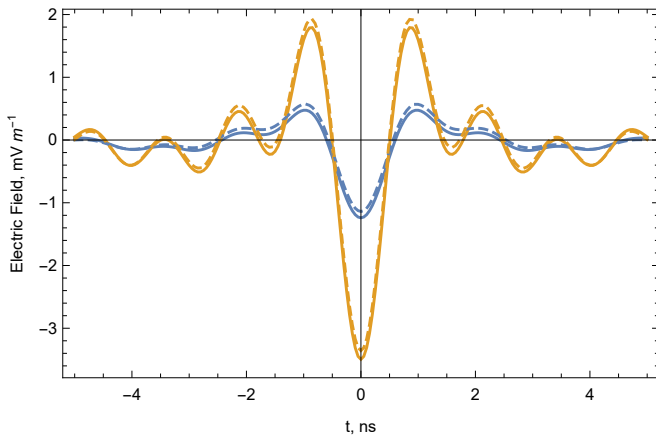


FIG. 4. Time-dependent electric field from Eq. (17) with $\theta = 0$, $\mathcal{R} = 35$ km, and $N = 5 \cdot 10^8$, using an idealized rectangle filter. The Lorentz factor is chosen to be $\gamma = 10$ (blue) and 20 (orange). Solid: filter spanning (40-80) MHz and (200-800) MHz; dashed: (200-800) MHz.

follows:

$$\mathbf{E}(t) = -\epsilon_{\parallel} \frac{18}{\sqrt{3}\pi\rho} \frac{\gamma^4 N e}{\mathcal{R}} \operatorname{Re} \left[\int_{\xi_{\min}}^{\xi_{\max}} \xi e^{-ia\xi} K_{2/3}(\xi) d\xi \right] \quad (19)$$

where we assume $b(\omega)$ as an idealized rectangle filter, $a \equiv 3\gamma^3 ct/\rho$ and (ξ_{\min}, ξ_{\max}) are determined by corresponding values of ω_{\min} and ω_{\max} characterizing the filter $b(\omega)$. From (19) one can explicitly see that the typical time duration is determined by parameter

$$(a\xi) \approx 2\pi \Rightarrow \tau \approx (2-4) \text{ ns}, \quad (20)$$

and the combination $(a\xi)$ which is the phase entering (19) is indeed γ -independent for $\theta \ll \gamma^{-1}$.

The same formula (19) also shows that the absolute value of the field $\mathbf{E}(t)$ and time duration is mostly determined by the region of the largest values of ξ close to

ξ_{\max} , while the low energy portion of the spectrum does not play a role. We explicitly checked this feature by plotting on Fig. 4 the electric field $\mathbf{E}(t)$ with two different models for the filter. Solid line includes both filters spanning the low and high frequency modes, while the dashed line corresponds to a single filter describing exclusively high frequency modes. The difference between the two curves is negligible as claimed. Another property worth to be mentioned is that the absolute value of the field $\mathbf{E}(t)$ in the peak increases with extending the upper value for ω_{\max} to higher value (800 MHz on Fig. 4 versus 600 MHz on Fig 3). This is also expected behaviour as the integral (19) is saturated by the region of the largest values of ξ close to ξ_{\max} , as already mentioned.

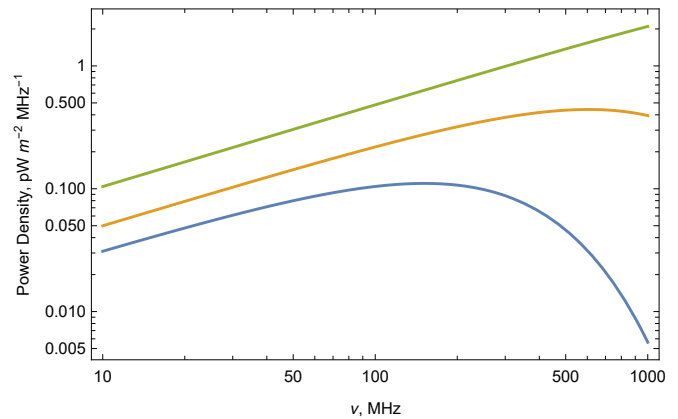


FIG. 5. Spectrum of power density from Eq. (24), with $\tau = 4$ ns, $\theta = 0$, $\mathcal{R} = 35$ km, and $N = 5 \cdot 10^8$. The Lorentz factor is chosen to be $\gamma = 10$ (blue), 20 (orange), and 60 (green).

The AQN-induced signal is in many aspects similar to the conventional CR shower, with crucial and dramatic difference being the *non-inverted polarity*. It well matches the observation of the anomalous events in ANITA experiment. We list a number of distinct features (between AQN-induced events and conventional CR air showers events) in concluding Sec. VI.

For completeness, we also derived the spectrum of power emission similar to the estimate in Ref. [83]. The power is related to the electric field by Poynting vector:

$$\mathbf{S}(t) = \frac{c}{4\pi} \mathbf{E}(t) \times \mathbf{B}(t) \quad (21)$$

where we use the Gaussian units. The power density is given by

$$\frac{dP(t)}{dA} = |\mathbf{S}(t)| = \frac{c}{4\pi} |\mathbf{E}(t)|^2. \quad (22)$$

Averaging over the time duration of the pulse τ , it gives

$$\left\langle \frac{dP(t)}{dA} \right\rangle_{\tau} = \frac{c}{4\pi\tau} \int |\mathbf{E}(t)|^2 dt \approx \frac{c}{4\pi\tau} \int |\mathbf{E}(\omega)|^2 d\omega. \quad (23)$$

where the last step follows from Parseval’s theorem. The spectrum of power density is therefore

$$\frac{d^2P}{d\omega dA} \approx \frac{d}{d\omega} \left\langle \frac{dP(t)}{dA} \right\rangle_{\tau} \approx \frac{c}{4\pi\tau} |\mathbf{E}(\omega)|^2. \quad (24)$$

The spectrum for the power of the emission shares similar properties as the one of electric field as it is expressed in terms of the electric field $|\mathbf{E}(\omega)|$. The results for the power density is presented on Fig. 5, where we use $\tau \approx 4$ ns for numerical estimates taken from (20), Fig 3 and Fig. 4. This value is also consistent with ANITA observations shown on Fig. 2 of Ref. [2]. The power density of order $(0.2 - 0.3)$ pW m⁻² MHz⁻¹ for $\gamma = 20$ and frequencies $\nu \gtrsim 100$ MHz, then it falls sharply beyond the critical frequency (16). This behaviour is consistent with ANITA’s results presented on Fig. 4 of Ref. [2].

We finish this section with few comments on accuracy of our estimates. It should be emphasized that the computations carried out in this section are oversimplified as realistic signals can be severely modified by numerous factors such as geometry of the beam, relative position of the observer, and frequency characteristic of the receiver’s filters [83, 84]. Nonetheless most factors, such as lateral structure and inclined axis of the beam, are near-field effects and they are eliminated since the observation angle is small. There are many other factors, such as the electron energy distribution of the beam as a function of γ , may modify our predictions. We cannot predict the corresponding behaviour as it is determined by very complex non-equilibrium dynamics as discussed in Appendix A. However, the basic features of the AQN-induced radio emission remain the same. In other words, the qualitative picture presented in this work cannot be dramatically modified as most AQN parameters used in the present estimates had been fixed by previous studies of numerous different and unrelated systems as reviewed in Sec. II.

VI. CONCLUSION AND FUTURE DEVELOPMENT

Our basic results can be summarized as follows. We argued that the two anomalous events observed by the ANITA collaboration [1–3] can be interpreted as the AQN-induced radio pulses which result from the AQN traversing the Earth and going in the upward direction. The basic qualitative characteristics (such as the frequency of emission, the strength of the electric field and the duration of the radio pulses as presented in previous section V) of the observed AAE are consistent with our proposal and this interpretation.

We also want to compare the results presented in this work with the studies of the conventional CR-induced radio emission [83, 84]. This comparison shows that the AQN-induced radio pulses can be easily discriminated from conventional sources, such as CR air showers.

But first, we start with similarities between CR-induced and the AQN-induced radio pulses. A “rule of thumb” suggests that the maximal number of charged particles (mostly electrons and positrons) in CR air shower is E_{CR}/GeV , which implies that $N \approx (10^8 - 10^9)$ for a $E_{\text{CR}} \approx (10^{17} - 10^{18})$ eV shower, see e.g. [83]. This number of electrons from CR shower is close to the number of electrons being emitted by the AQN according to (A11). Furthermore, the typical average energy in CR shower is 30 MeV which is also very similar to our estimates for the AQN-induced spectrum of the electrons with $E \in (1 - 10^2)$ MeV with the peak around 10 MeV according to (A11). Therefore, it should not be a surprise that the radio emission intensity and the strength of electric field is very similar in both cases as the geomagnetic field $B \approx 0.5$ gauss (which represents the source of the acceleration and consequent radio emission) is obviously the same in the same location.

Now we want to discuss the drastic differences between the pulses induced by conventional CR showers and the AQNs. These dramatic distinct features can be tested in future experiments, such that our proposal can be discriminated from any other suggestions. We list below the following typical spectral features of the CR-induced radio pulses and contrast them with the AQN induced radio pulses:

1. The generic spectral feature of the CR-induced radio emission is the presence of oscillations which normally start around 100 MHz (depending on the distance from the shower axis), see e.g. Fig. 1 in [84]. These oscillations are due to the coherence diminishing as the wavelength becomes shorter (in comparison to the “pancake” size in CR shower). While it is obviously affected by the detector’s filter, this feature is a physical effect due to changing number of coherent particles with different wavelengths. Such picture being typical for the CR-induced radio emission is not expected to occur for the AQN-induced radio signal as the notion of a “pancake” does not exist in our case, see also item 3 below with an argument that the notion of a “central axis” also does not exist for the AQN-induced events.

2. Another typical feature of the CR-induced radio emission is that the most of the power is emitted at frequencies around $(20 - 30)$ MHz for $E_{\text{CR}} \approx 10^{17}$ eV shower, see Fig. 2 in [84]. It is a result of very strong cutoff frequency $\nu_0 \lesssim 50$ MHz which strongly depends on features of the shower, see Eq. (2) and (12) in [84]. It should be contrasted with our case when the cutoff frequency $\nu_c \sim 0.7$ GHz is determined by dramatically different physics as expressed by (16).

3. Final and the most important difference between these two cases is that cutoff frequency ν_0 in CR air showers strongly depends on many parameters of the shower such as distance from the central axis when number of particles per unit area strongly depends on this parameter. It must be contrasted with our case of the AQN-induced radio signal when all electrons emitted from the same point at the same instant are moving along the same

direction.

This picture suggests that the event could be viewed as a uniform front of size $\rho \sim 0.8$ km defined by (11) rather than a CR air shower with a well defined central axis. In different words, the number of particles per unit area in the bunch of electrons does not depend on the distance from the central axis, in huge contrast with conventional CR air showers. The notion “central axis” simply does not exist for the AQN induced electrons as the number of particles per unit area is approximately the same for all electrons generating the radio pulse.

These features of the AQN-induced radio events are very distinct from conventional CR induced radio pulses, and it should be easily discriminated by future analysis with more quality data. It can be achieved, for example, by placing two or more independent but synchronized antennas at a distance to study the same events from different locations. If future studies indeed support and substantiate our proposal it would be a strong argument supporting the AQN nature of the AAEs.

We conclude with few comments on the possibility to test the AQN model with other instruments (in addition to the TA experiment mentioned previously in Section II B) such as the Pierre Auger Observatory and several projects of the Joint Experiment Missions for Extreme Universe Space Observatory (JEM-EUSO), including the currently operating Mini-EUSO detector, the planned EUSO on a Super Pressure Balloon II Mission (EUSO-SPB2), and the future Probe Of Extreme Multi-Messenger Astrophysics (POEMMA). As advocated recently, these instruments can potentially detect the UV photons from direct interaction between atmospheric molecules and macroscopic DMs (such as the AQN) [85, 86] or ultrahigh energy DMs [87].

Our original comments related to these studies are as follow. First, detection of macroscopically large quark nuggets, such as the AQNs, would require proper adjustment of bin time of detectors as argued in Ref. [85]. Furthermore, the AQN mostly emits photons in X ray bands, such that a signal cannot be observed by a fluorescence detector which is designed to detect the visible and UV light¹⁰. Finally, the X ray network suggested in [70] is capable to detect the X rays from the AQNs, and even determine the directionality and velocity distribution of the DM. It gives a real opportunity to test the Standard Halo Model (SHM) locally, which is known may dramatically deviate from conventional picture. This is because the standard parameters of the SHM are properly fixed only on the global (not local) scales, see Introduction in [70] for references and the details. We conclude with this optimistic note.

¹⁰ In fact, it was precisely the argument presented in [68] why the all sky camera has not observed any signal from a powerful meteor-like event detected by the infra-sound dedicated instrument.

ACKNOWLEDGEMENTS

This research was supported in part by the Natural Sciences and Engineering Research Council of Canada, and X.L. also by the UBC four year doctoral fellowship.

Appendix A: Some technical details on the AQN properties.

In this Appendix we want to make the estimates of the parameters which enter the formulae in the main body of the text. We want to estimate parameters such as mean free path λ , typical distance r^* where e^+e^- mostly produced, typical electric field and electric potential at distance r^* , etc.

We start our analysis with numerical estimate of the positron density for sufficiently large r when 1D expression (5) which is justified for $z \ll R$ does not apply at distance $r \gtrsim R$ as excited positrons will be far away from the core, i.e. at distances $r \gg R$.

We assume that the density $n(r, T)$ has a power-like behaviour at $r \gtrsim R$ with exponent p . This assumption is consistent with our numerical studies [79] of the electrosphere with $p \approx 6$. It is also consistent with conventional Thomas-Fermi model at $T = 0$, see e.g. Landau textbook¹¹. We keep parameter p to be arbitrary to demonstrate that our main claim is not very sensitive to our assumption on numerical value of p .

Therefore, we parameterize the density as follows

$$n(r, T) \approx n(z=0) \left(\frac{R}{r}\right)^p, \quad R \approx 2 \cdot 10^{-5} \text{cm} \quad (\text{A1})$$

$$n_0 \equiv n(z=0) \approx 0.16 \cdot 10^{31} \left(\frac{T}{100 \text{keV}}\right)^{\frac{3}{2}} \text{cm}^{-3}$$

where $n_0 \equiv n(z=0)$ is the positron density determined by the Eq. (6). The density profile (A1) allows us to estimate the effective charge of the nugget $Q_{\text{eff}}(r^*)$ at distance $r^* \gg R$ assuming that $Q_{\text{eff}}(r^*)$ is much greater than the number of positrons which completely left the system¹². The corresponding $Q_{\text{eff}}(r^*)$ can be estimated by integrating from r^* to infinity instead of accounting for the cancellations between the original negative charge of the antinugget and positive charge of the surrounding

¹¹ In notations of Ref. [88] the dimensionless function $\chi(x)$ behaves as $\chi \sim x^{-3}$ at large x . The potential $\phi = \chi(x)/x$ behaves as $\phi \sim x^{-4}$. The density of electrons in Thomas-Fermi model scales as $n \sim \phi^{3/2} \sim x^{-6}$ at large x .

¹² This assumption is essentially equivalent to the expectation that the positrons which completely left the system were localized at much larger distances, which is indeed the case. For example, the corresponding scale $R_{\text{cap}} \approx 1$ cm from [74] is indeed much greater than the scale $r^* \approx 10^{-3}$ cm which is the relevant scale of the problem to be discussed in this work.

positrons, i.e.

$$Q_{\text{eff}}(r^*) \approx \int_{r^*}^{\infty} 4\pi r^2 n(r) dr \sim \frac{4\pi n_0 R^3}{(p-3)} \left(\frac{R}{r^*}\right)^{p-3} \quad (\text{A2})$$

$$\approx 10^{11} \left(\frac{2 \cdot 10^{-3} \text{cm}}{r^*}\right)^3 \quad \text{for } p \approx 6.$$

In estimate (A2) we assumed that the power behaviour (A1) holds in this regime. The relevant parameter to consider is the charge to mass ratio Q_{eff}/M which is 14 orders of magnitude smaller for the AQNs in comparison with a similar ratio e/m_p computed for the proton. Indeed, the AQN's mass is of order $M \approx m_p B$ with a typical baryon charge $B \sim 10^{25}$, while $Q_{\text{eff}} \sim 10^{11}$.

Our next task is to estimate the binding energy $U(r^*)$ of the positrons at the distance r^* as follows:

$$U(r^*) = \frac{\alpha Q_{\text{eff}}(r^*)}{r^*} \approx 10 \text{ MeV} \left(\frac{2 \cdot 10^{-3} \text{cm}}{r^*}\right)^4. \quad (\text{A3})$$

This estimate suggests that if an electron will be created at distance $r^* \approx 2 \cdot 10^{-3} \text{cm}$ it will be quickly accelerated up to the energies of order 10 MeV as a result of strong repulsion due to the Coulomb force (A3). These parameters are used in an estimate in the main text in section III. To make our arguments more convincing we have to estimate a number of effects related to this physics. In particular, we have to estimate the rate of e^+e^- production at this distance r^* , the electron's mean free path $\lambda(r^*)$, the screening length, the equilibration time, and many other characteristics which support our proposal that the liberated electrons can generate, in principle, the anomalous radio pulse observed by ANITA.

We start with the estimation of the e^+e^- density in the environment at temperature T assuming that thermal equilibrium conditions are fulfilled. The corresponding density of the electrons n_- and positrons n_+ is given by conventional Fermi distribution [89]:

$$n_+ = n_- = \frac{1}{\pi^2} \int_0^{\infty} \frac{p^2 dp}{e^{\epsilon/T} + 1}, \quad \epsilon = \sqrt{p^2 + m^2}, \quad (\text{A4})$$

where the much smaller background positron's density $n(r^*)$ from (A1) has been ignored in the estimates (A4). For very low temperatures T the corresponding densities are exponentially small $\exp(-m/T)$ which simply reflects the fact that the number density of energetic photons which are capable to produce massive particles $\gamma\gamma \rightarrow e^+e^-$ is exponentially small.

Formula (A4) of course is valid only in large volume limit when all mean free paths for all processes are much smaller than the size of the system V such that the thermal equilibrium can be maintained. This condition is not satisfied however in our case of small nugget as we argue below.

Indeed, typical cross sections for $\gamma\gamma \rightarrow e^+e^-$ along with $e^+e^- \rightarrow \gamma\gamma$ and $\gamma e^{\pm} \rightarrow \gamma e^{\pm}$ at typical relativistic velocities corresponding to $T \approx 100 \text{ keV}$ and relevant for

the maintaining the thermal equilibrium are of order

$$\sigma_{\gamma\gamma \rightarrow e^+e^-} \sim \sigma_{e^+e^- \rightarrow \gamma\gamma} \sim \sigma_{\gamma e^{\pm} \rightarrow \gamma e^{\pm}} \sim \pi r_0^2, \quad (\text{A5})$$

$$r_0 = \frac{\alpha}{m} \approx 2.8 \cdot 10^{-13} \text{ cm}.$$

The mean free path for these processes can be estimated as follows

$$\lambda \sim \frac{1}{\sigma n_{\pm}} \sim 2.5 \cdot 10^{-3} \text{ cm}, \quad (\text{A6})$$

which is larger than the scale r^* entering Eqs. (A2) and (A3). This observation obviously implies that the thermal equilibrium cannot be maintained in such small volume of order $V \sim (r^*)^3$. Another process which equilibrates the system is the Coulomb elastic scattering with cross section σ_{Coul} estimated as follows:

$$\sigma_{\text{Coul}} \approx \frac{\alpha^2}{E^2 \theta^4} \approx 0.8 \cdot 10^{-25} \left(\frac{1}{\theta}\right)^4 \left(\frac{m}{E}\right)^2 \text{ cm}^2, \quad (\text{A7})$$

which is essentially the same order of magnitude as (A5) for $\theta \sim 1$. Furthermore, the processes related to σ_{Coul} as well as $\sigma_{e^+e^- \rightarrow \gamma\gamma}$ and $\sigma_{\gamma e^{\pm} \rightarrow \gamma e^{\pm}}$ decrease at large energies as E^{-2} as explicitly shown in (A7), which makes typical λ estimated in (A6) much greater at larger energies:

$$\lambda(E) \sim \frac{1}{\sigma(E) n_{\pm}} \sim 8 \cdot 10^{-3} \left(\frac{E}{m}\right)^2 \text{ cm}. \quad (\text{A8})$$

We mention dependence $\lambda(E)$ on energy E because the key element of our proposal is the fast acceleration of the produced electrons due to the strong background repulsive (for electrons) electric field determined by (A3). Our estimates presented above strongly suggest that the electrons produced by this mechanism can get accelerated up to 10 MeV energy without much scattering on the way as $\lambda(E)$ is very large in comparison with accelerating region of order $r^* \sim 10^{-3} \text{ cm}$.

Similar arguments also suggest that there is a suppression factor $(r^*/\lambda)^3 \ll 1$ which accounts for the ‘‘reduced’’ equilibration volume due to violation the basic requirement for the maintaining of the thermodynamical equilibrium as $\lambda \gg r^*$. There is an additional suppression related to dramatically different time scales: the typical time for the equilibration is λ/c is much longer than the typical time of electron's acceleration to relativistic velocity which is $t_0 \sim mr^*/U(r^*)$. After this short period of time t_0 the accelerated electrons are lost for the equilibration with other particles. Accounting for both these effects the maximal number of e^+e^- pairs being produced by this mechanism in volume $V \sim (r^*)^3$ can be estimated as follows:

$$[n_{\pm} \cdot V] \cdot \left(\frac{r^*}{\lambda}\right)^3 \cdot \left(\frac{t_0 c}{\lambda}\right) \sim 10^{15}, \quad V \sim (r^*)^3. \quad (\text{A9})$$

Another possible suppression factor could be due to a strong overestimation of the effective volume in (A9) approximated as $V \sim (r^*)^3$. The point is that the γ radiation and accompanied pair production of e^+e^- from

this region becomes the dominant cooling mechanism¹³ only in vicinity where quark and antiquark from AQNs get annihilated, which is determined by small area πR^2 . The equilibration time λ/c is too long to distribute this heat over entire volume $V \sim (r^*)^3$ sufficiently quickly before the particles leave the system. Therefore, we expect an additional suppression factor in (A9) which accounts for this effect:

$$\left(\frac{R}{r^*}\right)^2 \sim 10^{-4}. \quad (\text{A10})$$

Accounting for this additional suppression further reduces the estimate (A9) for the maximal number of available electrons:

$$N_{\max} \sim [n_{\pm} \cdot V] \left(\frac{r^*}{\lambda}\right)^3 \left(\frac{t_0 c}{\lambda}\right) \left(\frac{R}{r^*}\right)^2 \sim 10^{11}. \quad (\text{A11})$$

In addition to these suppression factors, there is a number of many-body effects which may modify the estimate (A11). For example, there is the Debye screening with the corresponding length λ_D being defined by the formula

$$\lambda_D \approx \sqrt{\frac{T}{4\pi\alpha n(r, T)}}, \quad (\text{A12})$$

where $n(r, T)$ is the background positron density determined by (A1).

The Debye screening normally applies to the situation when a single external charge q is inserted into the plasma. In this case the charge q will be screened on the scale λ_D , i.e. $q \exp(-r^*/\lambda_D)$. There are few assumptions for the Debye screening to be operational. First of all the elementary processes responsible for the screening should be much faster than the typical time scales of a slowly moving external charge q . Secondly, the density of the external charges q must be much smaller than the density of the charged particles in surrounding plasma. Both assumptions are not justified in our case when we treat the produced electrons as the inserted external charges. The density (A4) of the e^+e^- pairs (which are treated as external charges) is also greater than background density (A1) at distance r^* . Therefore, we do not expect that the Debye screening is operational in the present

circumstances, and we ignored it in our order of magnitude estimate (A11).

One should also mention that the density of photons n_γ at this temperature T in this region is much higher than the density of e^+e^- pairs (A4) by at least factor of $\exp(m/T)$. These photons with typical frequencies $\omega \sim T$ may leave the system. In fact, they provide the dominant cooling mechanism in atmosphere as we already mentioned in the main text. However, we are not interested in the fate of these photons in the present work as they will be quickly absorbed on relatively short distances from the AQN's path.

All these arguments with numerous suppression factors entering (A11), show a huge uncertainty in the estimates for effective number of electrons N which are capable to get accelerated to 10 MeV energies, leave the system, and consequently propagate for several kilometers, which is the mean free path in atmosphere for such energetic electrons. Therefore, in the main body of the text we treat the number of accelerated electrons at the moment when the AQN just crosses the earth surface and enters the atmosphere as free parameter $N \ll N_{\max}$. Precise estimate is very hard to make as it is a prerogative of the non-equilibrium dynamics, the topic which is well beyond the scope of the present work.

One may wonder why we choose the key scale of the problem to be $r^* \approx 10^{-3}$ cm and not much smaller or much greater than this scale. The answer is as follows. If we take much smaller scale, let us say one order of magnitude smaller than $r^* \approx 10^{-3}$ cm, the typical number of particles N_{\max} would be 4 orders of magnitude fewer than the estimate (A11). On other hand if we take much greater scale, let us say few times larger than $r^* \approx 10^{-3}$ cm we would get electric field (A3) to be too weak to accelerate the particles to sufficiently high energies when they can leave the system without much re-scattering and eventual annihilation with surrounding positrons. In general one should expect that there will be entire spectrum of the accelerated particles in the range $E \in (1 - 10^2)$ MeV which are capable to leave the system. However, for our qualitative studies we assume that the peak of this distribution is somewhere around the 10 MeV scale, i.e.

$$\langle E \rangle \sim U(r^*) \sim 10 \text{ MeV}, \quad E \in (1 - 10^2) \text{ MeV}, \quad (\text{A13})$$

which is precisely the magnitude we used in all our estimates in the main body of the text.

[1] P. W. Gorham *et al.* (ANITA), *Phys. Rev. Lett.* **117**, 071101 (2016), [arXiv:1603.05218 \[astro-ph.HE\]](#).

[2] P. W. Gorham *et al.* (ANITA), *Phys. Rev. Lett.* **121**, 161102 (2018), [arXiv:1803.05088 \[astro-ph.HE\]](#).

[3] P. W. Gorham *et al.* (ANITA), (2020), [arXiv:2008.05690 \[astro-ph.HE\]](#).

[4] P. Motloch, J. Alvarez-Muñiz, P. Privitera, and E. Zas, *Phys. Rev. D* **95**, 043004 (2017), [arXiv:1606.07059 \[astro-ph.HE\]](#).

[5] D. B. Fox, S. Sigurdsson, S. Shandera, P. Mészáros,

¹³ The dominant cooling mechanism for relatively low temperature T is determined by emission from electrosphere as discussed in [78].

- K. Murase, M. Mostafá, and S. Coutu, (2018), [arXiv:1809.09615 \[astro-ph.HE\]](#).
- [6] A. Romero-Wolf *et al.*, *Phys. Rev. D* **99**, 063011 (2019), [arXiv:1811.07261 \[astro-ph.HE\]](#).
- [7] B. Chauhan and S. Mohanty, *Phys. Rev. D* **99**, 095018 (2019), [arXiv:1812.00919 \[hep-ph\]](#).
- [8] P. Dasgupta and P. Jain, *Astropart. Phys.* **128**, 102530 (2021), [arXiv:1811.00900 \[physics.class-ph\]](#).
- [9] L. Heurtier, Y. Mambrini, and M. Pierre, *Phys. Rev. D* **99**, 095014 (2019), [arXiv:1902.04584 \[hep-ph\]](#).
- [10] K. D. de Vries and S. Prohira, *Phys. Rev. Lett.* **123**, 091102 (2019), [arXiv:1903.08750 \[astro-ph.HE\]](#).
- [11] D. Hooper, S. Wegsman, C. Deaconu, and A. Viereg, *Phys. Rev. D* **100**, 043019 (2019), [arXiv:1904.12865 \[astro-ph.HE\]](#).
- [12] J. M. Cline, C. Gross, and W. Xue, *Phys. Rev. D* **100**, 015031 (2019), [arXiv:1904.13396 \[hep-ph\]](#).
- [13] I. M. Shoemaker, A. Kusenko, P. K. Munneke, A. Romero-Wolf, D. M. Schroeder, and M. J. Siegert, *Annals Glaciol.* **61**, 92 (2020), [arXiv:1905.02846 \[astro-ph.HE\]](#).
- [14] L. A. Anchordoqui *et al.*, *PoS ICRC2019*, 884 (2020), [arXiv:1907.06308 \[hep-ph\]](#).
- [15] D. Smith *et al.*, (2020), [arXiv:2009.13010 \[astro-ph.HE\]](#).
- [16] L. A. Anchordoqui, V. Barger, J. G. Learned, D. Marfatia, and T. J. Weiler, *LHEP* **1**, 13 (2018), [arXiv:1803.11554 \[hep-ph\]](#).
- [17] E. Dudas, T. Gherghetta, K. Kaneta, Y. Mambrini, and K. A. Olive, *Phys. Rev. D* **98**, 015030 (2018), [arXiv:1805.07342 \[hep-ph\]](#).
- [18] G.-y. Huang, *Phys. Rev. D* **98**, 043019 (2018), [arXiv:1804.05362 \[hep-ph\]](#).
- [19] A. Connolly, P. Allison, and O. Banerjee, (2018), [arXiv:1807.08892 \[astro-ph.HE\]](#).
- [20] J. F. Cherry and I. M. Shoemaker, *Phys. Rev. D* **99**, 063016 (2019), [arXiv:1802.01611 \[hep-ph\]](#).
- [21] L. A. Anchordoqui and I. Antoniadis, *Phys. Lett. B* **790**, 578 (2019), [arXiv:1812.01520 \[hep-ph\]](#).
- [22] J. H. Collins, P. S. Bhupal Dev, and Y. Sui, *Phys. Rev. D* **99**, 043009 (2019), [arXiv:1810.08479 \[hep-ph\]](#).
- [23] L. Heurtier, D. Kim, J.-C. Park, and S. Shin, *Phys. Rev. D* **100**, 055004 (2019), [arXiv:1905.13223 \[hep-ph\]](#).
- [24] S. Chipman, R. Dising, M. H. Reno, and I. Sarcevic, *Phys. Rev. D* **100**, 063011 (2019), [arXiv:1906.11736 \[astro-ph.HE\]](#).
- [25] M. Abdullah, B. Dutta, S. Ghosh, and T. Li, *Phys. Rev. D* **100**, 115006 (2019), [arXiv:1907.08109 \[hep-ph\]](#).
- [26] D. Borah, A. Dasgupta, U. K. Dey, and G. Tomar, *Phys. Rev. D* **101**, 075039 (2020), [arXiv:1907.02740 \[hep-ph\]](#).
- [27] A. Esmaili and Y. Farzan, *JCAP* **12**, 017 (2019), [arXiv:1909.07995 \[hep-ph\]](#).
- [28] I. Esteban, J. Lopez-Pavon, I. Martinez-Soler, and J. Salvado, *Eur. Phys. J. C* **80**, 259 (2020), [arXiv:1905.10372 \[hep-ph\]](#).
- [29] W. Altmannshofer, P. S. B. Dev, A. Soni, and Y. Sui, *Phys. Rev. D* **102**, 015031 (2020), [arXiv:2002.12910 \[hep-ph\]](#).
- [30] M. G. Aartsen *et al.* (IceCube), (2020), [10.3847/1538-4357/ab791d](#), [arXiv:2001.01737 \[astro-ph.HE\]](#).
- [31] A. R. Zhitnitsky, *JCAP* **10**, 010 (2003), [hep-ph/0202161](#).
- [32] E. Witten, *Phys. Rev. D* **30**, 272 (1984).
- [33] E. Farhi and R. L. Jaffe, *Phys. Rev. D* **30**, 2379 (1984).
- [34] A. De Rújula and S. L. Glashow, *Nature (London)* **312**, 734 (1984).
- [35] J. Madsen, in *Hadrons in Dense Matter and Hadrosynthesis*, Lecture Notes in Physics, Berlin Springer Verlag, Vol. 516, edited by J. Cleymans, H. B. Geyer, and F. G. Scholtz (1999) p. 162, [astro-ph/9809032](#).
- [36] R. D. Peccei and H. R. Quinn, *Phys. Rev. D* **16**, 1791 (1977).
- [37] S. Weinberg, *Phys. Rev. Lett.* **40**, 223 (1978).
- [38] F. Wilczek, *Phys. Rev. Lett.* **40**, 279 (1978).
- [39] J. E. Kim, *Phys. Rev. Lett.* **43**, 103 (1979).
- [40] M. A. Shifman, A. I. Vainshtein, and V. I. Zakharov, *Nucl. Phys. B* **166**, 493 (1980).
- [41] M. Dine, W. Fischler, and M. Srednicki, *Phys. Lett. B* **104**, 199 (1981).
- [42] A. R. Zhitnitsky, *Sov. J. Nucl. Phys.* **31**, 260 (1980), [*Yad. Fiz.*31,497(1980)].
- [43] K. Van Bibber and L. J. Rosenberg, *Physics Today* **59**, 30 (2006).
- [44] S. J. Asztalos, L. J. Rosenberg, K. van Bibber, P. Sikivie, and K. Zioutas, *Annual Review of Nuclear and Particle Science* **56**, 293 (2006).
- [45] P. Sikivie, in *Axions*, Lecture Notes in Physics, Berlin Springer Verlag, Vol. 741, edited by M. Kuster, G. Raffelt, and B. Beltrán (2008) p. 19, [astro-ph/0610440](#).
- [46] G. G. Raffelt, in *Axions*, Lecture Notes in Physics, Berlin Springer Verlag, Vol. 741, edited by M. Kuster, G. Raffelt, and B. Beltrán (2008) p. 51, [hep-ph/0611350](#).
- [47] P. Sikivie, *International Journal of Modern Physics A* **25**, 554 (2010), [arXiv:0909.0949 \[hep-ph\]](#).
- [48] L. J. Rosenberg, *Proceedings of the National Academy of Science* **112**, 12278 (2015).
- [49] D. J. E. Marsh, *Phys. Rep.* **643**, 1 (2016), [arXiv:1510.07633](#).
- [50] P. W. Graham, I. G. Irastorza, S. K. Lamoreaux, A. Lindner, and K. A. van Bibber, *Annual Review of Nuclear and Particle Science* **65**, 485 (2015), [arXiv:1602.00039 \[hep-ex\]](#).
- [51] I. G. Irastorza and J. Redondo, *Prog. Part. Nucl. Phys.* **102**, 89 (2018), [arXiv:1801.08127 \[hep-ph\]](#).
- [52] X. Liang and A. Zhitnitsky, *Phys. Rev. D* **94**, 083502 (2016), [arXiv:1606.00435 \[hep-ph\]](#).
- [53] S. Ge, X. Liang, and A. Zhitnitsky, *Phys. Rev. D* **96**, 063514 (2017), [arXiv:1702.04354 \[hep-ph\]](#).
- [54] S. Ge, X. Liang, and A. Zhitnitsky, *Phys. Rev. D* **97**, 043008 (2018), [arXiv:1711.06271 \[hep-ph\]](#).
- [55] S. Ge, K. Lawson, and A. Zhitnitsky, *Phys. Rev. D* **99**, 116017 (2019), [arXiv:1903.05090 \[hep-ph\]](#).
- [56] E. N. Parker, *Astrophys. J.* **330**, 474 (1988).
- [57] S. Mondal, D. Oberoi, and A. Mohan, *Astrophys. J.* **895**, L39 (2020).
- [58] A. Zhitnitsky, *JCAP* **10**, 050 (2017), [arXiv:1707.03400 \[astro-ph.SR\]](#).
- [59] N. Raza, L. van Waerbeke, and A. Zhitnitsky, *Phys. Rev. D* **98**, 103527 (2018), [arXiv:1805.01897 \[astro-ph.SR\]](#).
- [60] S. Ge, M. S. R. Siddiqui, L. Van Waerbeke, and A. Zhitnitsky, *Phys. Rev. D* **102**, 123021 (2020), [arXiv:2009.00004 \[astro-ph.HE\]](#).
- [61] D. M. Jacobs, G. D. Starkman, and B. W. Lynn, *Mon. Not. Roy. Astron. Soc.* **450**, 3418 (2015), [arXiv:1410.2236 \[astro-ph.CO\]](#).
- [62] K. Lawson, X. Liang, A. Mead, M. S. R. Siddiqui, L. Van Waerbeke, and A. Zhitnitsky, *Phys. Rev. D* **100**, 043531 (2019), [arXiv:1905.00022 \[astro-ph.CO\]](#).
- [63] P. W. Gorham, *Phys. Rev. D* **86**, 123005 (2012), [arXiv:1208.3697 \[astro-ph.CO\]](#).

- [64] P. W. Gorham and B. J. Rotter, *Phys. Rev. D* **95**, 103002 (2017), [arXiv:1507.03545 \[astro-ph.CO\]](#).
- [65] K. Lawson and A. R. Zhitnitsky, *Phys. Rev. D* **95**, 063521 (2017), [arXiv:1510.07646 \[astro-ph.HE\]](#).
- [66] A. Zhitnitsky, *Phys. Rev. D* **101**, 083020 (2020), [arXiv:1909.05320 \[hep-ph\]](#).
- [67] J. Singh Sidhu, R. J. Scherrer, and G. Starkman, *Phys. Lett. B* **807**, 135574 (2020), [arXiv:2006.01200 \[astro-ph.CO\]](#).
- [68] D. Budker, V. V. Flambaum, and A. Zhitnitsky, (2020), [arXiv:2003.07363 \[hep-ph\]](#).
- [69] D. Budker, V. V. Flambaum, X. Liang, and A. Zhitnitsky, *Phys. Rev. D* **101**, 043012 (2020), [arXiv:1909.09475 \[hep-ph\]](#).
- [70] X. Liang, E. Peshkov, L. Van Waerbeke, and A. Zhitnitsky, *Phys. Rev. D* **103**, 096001 (2021), [arXiv:2012.00765](#).
- [71] N. L. Figueroa, D. Budker, and E. M. Rasel, (2021), [arXiv:2103.08715 \[astro-ph.CO\]](#).
- [72] R. Abbasi *et al.* (Telescope Array Project), *Phys. Lett. A* **381**, 2565 (2017).
- [73] T. Okuda, *Journal of Physics: Conference Series* **1181**, 012067 (2019).
- [74] A. Zhitnitsky, *J. Phys. G* **48**, 065201 (2021), [arXiv:2008.04325 \[hep-ph\]](#).
- [75] X. Liang and A. Zhitnitsky, (2021), [arXiv:2101.01722 \[hep-ph\]](#).
- [76] G. W. Fraser, A. M. Read, S. Sembay, J. A. Carter, and E. Schyns, *Mon. Not. Roy. Astron. Soc.* **445**, 2146 (2014), [arXiv:1403.2436 \[astro-ph.HE\]](#).
- [77] S. Ge, H. Rachmat, M. S. R. Siddiqui, L. Van Waerbeke, and A. Zhitnitsky, (2020), [arXiv:2004.00632 \[astro-ph.HE\]](#).
- [78] M. M. Forbes and A. R. Zhitnitsky, *Phys. Rev. D* **78**, 083505 (2008), [arXiv:0802.3830](#).
- [79] M. M. Forbes, K. Lawson, and A. R. Zhitnitsky, *Phys. Rev. D* **82**, 083510 (2010), [arXiv:0910.4541](#).
- [80] H. Schoorlemmer *et al.*, *Astropart. Phys.* **77**, 32 (2016), [arXiv:1506.05396 \[astro-ph.HE\]](#).
- [81] X. Liang, A. Mead, M. S. R. Siddiqui, L. Van Waerbeke, and A. Zhitnitsky, *Phys. Rev. D* **101**, 043512 (2020), [arXiv:1908.04675 \[astro-ph.CO\]](#).
- [82] J. D. Jackson, *Classical electrodynamics*, 3rd ed. (Wiley, New York, NY, 1999).
- [83] T. Huege and H. Falcke, *Astron. Astrophys.* **412**, 19 (2003), [arXiv:astro-ph/0309622](#).
- [84] T. Huege and H. Falcke, *Astroparticle Physics* **24**, 116 (2005).
- [85] J. Singh Sidhu, R. M. Abraham, C. Covault, and G. Starkman, *JCAP* **02**, 037 (2019), [arXiv:1808.06978 \[astro-ph.HE\]](#).
- [86] L. A. Anchordoqui *et al.*, (2021), [arXiv:2104.05131 \[hep-ph\]](#).
- [87] Y. Xu, *Publ. Astron. Soc. Jap.* **73**, 365 (2021), [arXiv:1910.11158 \[astro-ph.HE\]](#).
- [88] L. D. Landau and E. M. Lifshitz, *Quantum Mechanics, 3rd edition* (Butterworth-Heinemann, Oxford, 1977).
- [89] L. D. Landau and E. M. Lifshitz, *Statistical Physics, Part-1, 3rd edition* (Butterworth-Heinemann, Oxford, 1977).